Photoinduced Energy and Electron Transfer Processes in Supramolecular Species. Tris(bipyridine) Complexes of Ru(II)/Os(II), Ru(II)/Ru(III), Os(II)/Os(III), and Ru(II)/Os(III) Separated by a Rigid Spacer

Luisa De Cola,*[1a] Vincenzo Balzani,*[1a] Francesco Barigelletti,[1b] Lucia Flamigni,[1b] Peter Belser,*[1c] Alex von Zelewsky,[1c] Michael Frank,[1d] and Fritz Vögtle*[1d]

Dipartimento di Chimica "G. Ciamician" dell'Università and Istituto FRAE-CNR, Bologna, Italy, Institut für Anorganische Chemie, Universität Freiburg, Freiburg, Switzerland, and Institut für Organische Chemie und Biochemie, Universität Bonn, Bonn, Germany

*Received June 9, 1993**

The bis(bipyridine) bridging ligand 1,4-bis[2-(2,2'-bipyridin-5-yl)ethenyl]bicyclo[2.2.2]octane (bpy–S–bpy), where S is a rigid spacer made of a bicyclooctane unit symmetrically linked to two ethylene-type units in a *E*,*E*-configuration, has been synthesized and its complexes $(bpy)_2Ru(bpy–S–bpy)^{2+}$ (Ru^{II}·A), $(bpy)_2Os(bpy–S–bpy)^{2+}$ (Os^{II}·A), $(bpy)_2Ru(bpy–S–bpy)Ru(bpy)_2^{4+}$ (Ru^{II}·A·Ru^{II}), $(bpy)_2Os(bpy–S–bpy)Os(bpy)_2^{4+}$ (Os^{II}·A·Os^{II}), $(bpy)_2Ru(bpy–S–bpy)Os(bpy)_2^{4+}$ (Ru^{II}·A·Os^{II}) have been prepared as PF_6^- salts. The length of the rigid spacer S is 9 Å, and the center-to-center separation distance in the dinuclear complexes is 17 Å. In all these novel compounds, each Ru-based and Os-based unit displays its own absorption spectrum and electrochemical properties, regardless of the presence of a second metal-based unit. The homometallic dinuclear compounds exhibit the same luminescence properties as the corresponding mononuclear species, whereas in the heterometallic dinuclear Ru^{II}·A·Os^{II} species 91% of the Ru-based luminescence intensity is quenched by energy transfer to the Os-based unit, whose luminescence is accordingly sensitized (acetonitrile solution, room temperature). The excited state lifetime of the Ru-based unit (209 ns) is reduced to 18 ns, and a comparable risetime is observed for the energy transfer sensitization of the Os-based luminescence. The energy transfer process occurs with rate constant 5.0×10^7 s^{-1}, predominantly by an exchange mechanism. Partial oxidation of the binuclear species Ru^{II}·A·Ru^{II}, Os^{II}·A·Os^{II}, and Ru^{II}·A·Os^{II} by Ce(IV) in acetonitrile–water solutions leads to mixed-valence M^{II}·A·M^{III} species (M = Ru and/or Os) where the oxidized metal-based unit quenches the luminescent excited state of the unit that is not oxidized. For the Ru^{II}·A·Os^{III} compound, the residual luminescent intensity of the Ru-based unit is <1.5% and its excited state lifetime is 115 ps. The quenching occurs by electron transfer ($k_{el} = 8.7 \times 10^9$ s^{-1}) with formation of the thermodynamically unstable Ru^{III}·A·Os^{II} valence isomer which then goes back ($k_b = 1.0 \times 10^6$ s^{-1}) to Ru^{II}·A·Os^{III}. The Ru^{II}·A·Ru^{III} and Os^{II}·A·Os^{III} mixed-valence compounds can only be obtained in the presence of the corresponding M^{II}·A·M^{II} and M^{III}·A·M^{III} species, according to a statistical distribution. For both the homometallic mixed-valence compounds the quenching of the luminescence intensity of the nonoxidized unit by the oxidized one is larger than 90%. Lifetime measurements have shown that the quenching rate constant is 1.1×10^9 s^{-1} for Ru^{II}·A·Ru^{III} and 5.0×10^9 s^{-1} for Os^{II}·A·Os^{III}. The quenching process takes place by an electron transfer mechanism. The parameters which govern the rates of the energy and electron transfer processes in this homogeneous family of compounds are discussed in the light of current theories. It is shown that the electronic matrix element is ~0.6 cm^{-1} for the energy transfer process in *Ru^{II}·A·Os^{II}, ~7–10 cm^{-1} for the electron transfer processes in *Ru^{II}·A·Os^{III}, *Ru^{II}·A·Ru^{III}, and *Os^{II}·A·Os^{III}, and ~1.0 cm^{-1} for the (back) electron transfer process in Ru^{III}·A·Os^{II}.

Introduction

Photoinduced energy and electron transfer processes lie at the heart of fundamental natural phenomena (e.g., photosynthesis)[2] as well as of a variety of applications.[3] In the last few years the research in this field has progressively moved from molecular to supramolecular systems,[4–13] with the dual purpose of testing current theoretical treatments[14–20] and designing nanoscale devices capable of performing useful light-induced functions.[5,21] A large

* Abstract published in *Advance ACS Abstracts*, October 1, 1993.

(1) (a) University of Bologna. (b) FRAE-CNR. (c) University of Fribourg. (d) University of Bonn.
(2) See, e.g.: Hader, D.-P.; Tevini, M. *General Photobiology*; Pergamon: Oxford, England, 1987.
(3) (a) Fox, M. A.; Chanon, M. Eds.: *Photoinduced Electron Transfer*; Elsevier: New York, USA, 1988; Part A–D. (b) Mattay, J., Ed.: *Top. Curr. Chem.* **1990**, *156*; **1990**, *158*; **1991**, *159*.
(4) Lehn, J. M. *Angew. Chem., Int. Ed. Engl.* **1988**, *27*, 89.
(5) Balzani, V.; Scandola, F. *Supramolecular Photochemistry*; Horwood: Chichester, U.K., 1991.
(6) Connolly, J. S.; Bolton, J. R. In *Photoinduced Electron Transfer*; Fox, M. A., Chanon, M., Eds.; Part D; Elsevier: New York, 1988; p 303.
(7) Wasielewski, M. R. In *Photoinduced Electron Transfer*; Fox, M. A.; Chanon, M., Eds.; Elsevier: New York, USA, 1988; Part D, p 161.
(8) Closs, G. L.; Miller, J. R. *Science* **1988**, *240*, 440.
(9) Gust, D.; Moore, T. A. *Science* **1989**, *244*, 35.
(10) Scandola, F.; Indelli, M. T.; Chiorboli, C.; Bignozzi, C. A. *Top. Curr. Chem.* **1990**, *158*, 73.
(11) Vögtle, F. *Supramolecular Chemistry*; Wiley: Chichester, U.K, **1991**.
(12) Balzani, V., De Cola, L., Eds.; *Supramolecular Chemistry*; Kluwer: Dordrecht, The Netherlands, 1992.
(13) Balzani, V., *Tetrahedron* **1992**, *48*, 10443.
(14) Marcus, R. A.; Sutin, N. *Biochim. Biophys. Acta* **1985**, *811*, 265.
(15) Jortner, J. *J. Chem. Phys.* **1976**, *64*, 4860.
(16) Orlandi, G.; Monti, S.; Barigelletti, F.; Balzani, V. *Chem. Phys.* **1980**, *52*, 313.
(17) Miller, J. R.; Beitz, J. V. *J. Chem. Phys.* **1981**, *74*, 6746.
(18) Oevering, H.; Paddon-Row, M. N.; Hoppener, M.; Oliver, A. M.; Cotsaris, E.; Verhoeven, J. W.; Hush, N. S. *J. Am. Chem. Soc.* **1987**, *109*, 3258.
(19) Closs, G. L.; Calcaterra, L. T.; Green, N. J.; Penfield, K. W.; Miller, J. R. *J. Phys. Chem.* **1986**, *90*, 3673.
(20) Wasielewski, M. R.; Niemczyk, M. P.; Johnson, D. G.; Svec, W. A.; Minsek, D. W. *Tetrahedron* **1989**, *45*, 4785.
(21) See, e.g.: (a) Hopfield, J. J.; Onuchic, J. N.; Beratan, D. N. *J. Phys. Chem.* **1989**, *93*, 6350. (b) O'Regan, B.; Graetzel, M. *Nature*, **1991**, *353*, 737. (c) Anelli, P. L.; Ashton, P. R.; Ballardini, R.; Balzani, V.; Delgado, M.; Gandolfi, M. T.; Goodnow, T. T.; Kaifer, A. E.; Philp, D.; Pietraszkiewicz, M.; Prodi, L.; Reddington, M. V.; Slawin, A. M. Z.; Spencer, N.; Stoddart, J. F.; Vicent, C.; Williams, D. J. *J. Am. Chem. Soc.* **1992**, *114*, 193. (d) Denti, G.; Campagna, S.; Balzani, V.; In *Mesomolecules: From Molecules to Materials*, Mendenhall, G. D.; Greenberg, A.; Liebman, J., Eds.; Chapman and Hall: New York, in press.

0020-1669/93/1332-5228$04.00/0

number of supramolecular species made of covalently linked building blocks have been recently investigated for these purposes.

Ru(II) and Os(II) polypyridine-type complexes[22] exhibit suitable excited-state and redox properties to play the role of building blocks for the construction of photoactive supramolecular systems.[5,10,23-42] For synthetic reasons, however, it is quite difficult to assemble these metal-containing building blocks in an extended, yet sufficiently rigid, supramolecular structure. As a consequence, in most cases the distance over which electron or energy transfer processes take place in such systems is only approximately known, and important pieces of information concerning the factors which determine the values of the rate constants of such processes are lost.

Continuing our studies in this field,[42] we have designed and synthesized the bis(bipyridine) bridging ligand 1,4-bis[2,2′-bipyridin-5-yl)ethenyl]bicyclo[2.2.2]octane (bpy–S–bpy, Figure 1) where the spacer (9-Å long), which separates the two chelating bpy sites, is made of a rigid bicyclooctane component linked to two ethylene-type units, each of which exhibits *E* geometrical configuration. Although rotation about the single C–C bonds which connect the ethylene units to the bpy ligands and to the central bicyclooctane unit can take place, in the dinuclear compounds the distance between the metal centers (which are separated by 15 bonds) is confined between 16 and 18 Å. By using this novel bridging ligand, we have synthesized the mononuclear complexes $(bpy)_2Ru(bpy–S–bpy)^{2+}$ (**Ru^{II}·A**) and $(bpy)_2Os(bpy–S–bpy)^{2+}$ (**Os^{II}·A**), and the dinuclear complexes

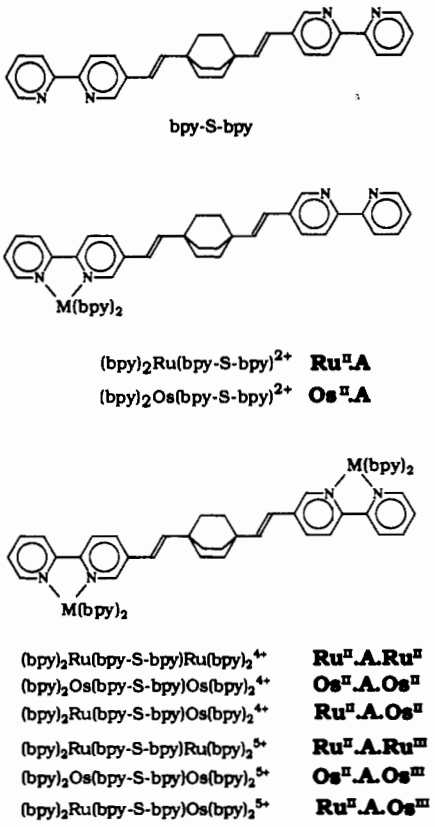

Figure 1. Schematic representation of the bridging ligand bpy–S–bpy and of its mononuclear and binuclear complexes. The abbrevations used to indicate the metal complexes are also shown.

$(bpy)_2Ru(bpy–S–bpy)Ru(bpy)_2^{4+}$ (**Ru^{II}·A·Ru^{II}**), $(bpy)_2Os(bpy–S–bpy)Os(bpy)_2^{4+}$ (**Os^{II}·A·Os^{II}**), and $(bpy)_2Ru(bpy–S–bpy)Os(bpy)_2^{4+}$ (**Ru^{II}·A·Os^{II}**) as PF_6^- salts. A schematic representation of the complexes is shown in Figure 1. We have characterized the spectroscopic, luminescence, and electrochemical properties of the mononuclear and dinuclear species, and we have investigated the quenching of the luminescence of the Ru-based unit by the Os-based one in the heterometallic **Ru^{II}·A·Os^{II}** species.[43] Then, we have oxidized in solution the dinuclear compounds to obtain the mixed-valence $(bpy)_2Ru(bpy–S–bpy)Ru(bpy)_2^{5+}$ (**Ru^{II}·A·Ru^{III}**), $(bpy)_2Os(bpy–S–bpy)Os(bpy)_2^{5+}$ (**Os^{II}·A·Os^{III}**), and $(bpy)_2Ru(bpy–S–bpy)Os(bpy)_2^{5+}$ (**Ru^{II}·A·Os^{III}**) species, where the luminescence of the Ru^{II}- or Os^{II}-based unit is quenched by the Ru^{III}- or Os^{III}-based one. The rate constants for the photoinduced energy or electron transfer processes have been measured and the results obtained have been discussed in the light of current theories.

Experimental Section

Equipment and Methods. Electrochemical measurements were carried out at room temperature (~25 °C) by using a PAR 273A Electrochemical Analysis System with the 270 Research Electrochemistry Software. Cyclic voltammograms were obtained in acetonitrile solution by using a microcell equipped with a stationary platinum disk electrode, a platinum disk counter electrode, and a SCE reference electrode with tetrabutylammonium hexafluorophosphate as supporting electrolyte. In all cases $[Ru(bpy)_3](PF_6)_2$ was used as a standard, taking its oxidation potential equal to +1260 mV vs SCE.[44] The electrochemical window examined was between +1.6 and −2.0 V. Scanning speed was 200 mV s^{-1}. All the reported values are *vs* SCE. Half-wave potentials were calculated as an average of the cathodic and anodic peaks.

(22) (a) Juris, A.; Balzani, V.; Barigelletti, F.; Campagna, S.; Belser, P.; von Zelewsky, A. *Coord. Chem. Rev.* **1988**, *84*, 85. (b) Kober, E. M.; Caspar, J. V.; Sullivan, B. P.; Meyer, T. J. *Inorg. Chem.* **1988**, *27*, 4587.
(23) For some recent papers, see refs 24–42.
(24) (a) Serroni, S.; Denti, G.; Campagna, S.; Juris, A.; Ciano, M.; Balzani, V. *Angew. Chem., Int. Ed. Engl.* **1993**, *31*, 1495. (b) Denti, G.; Campagna, S.; Serroni, S.; Ciano, M.; Balzani, V. *J. Am. Chem. Soc.* **1992**, *114*, 2944.
(25) Collin, J.-P.; Guillerez, S.; Sauvage, J.-P.; Barigelletti, F.; De Cola, L.; Flamigni, L.; Balzani, V. *Inorg. Chem.* **1992**, *31*, 4112.
(26) (a) Kalyanasundaram, K.; Grätzel, M.; Nazeeruddin, M. K. *J. Phys. Chem.* **1992**, *96*, 5865. (b) Matsui, K.; Nazeeruddin, M. K.; Humphry-Baker, R.; Grätzel, M.; Kalyanasundaram, K. *J. Phys. Chem.* **1992**, *96*, 10587.
(27) (a) Bignozzi, C. A.; Bortolini, O.; Chiorboli, C.; Indelli, M. T.; Rampi, M. A.; Scandola, F., *Inorg. Chem.* **1992**, *31*, 172. (b) Bignozzi, C. A.; Argazzi, R.; Garcia, C. G.; Scandola, F.; Schoonover, J. R.; Meyer, T. J. *J. Am. Chem. Soc.* **1992**, *114*, 8727.
(28) (a) Younathan, J. N.; Jones, W. E.; Meyer, T. J. *J. Phys. Chem.* **1991**, *95*, 488. (b) Murtaza, Z.; Zipp, A. P.; Worl, L. A.; Graff, D.; Jones, W. E.; Bates, W. D.; Meyer, T. J. *J. Chem. Soc.* **1991**, *113*, 5113. (c) Meckenburg, S. L.; Peek, B. M.; Erickson, B. W.; Meyer, T. J. *J. Am. Chem. Soc.* **1991**, *113*, 8540. (d) Worl, L. A.; Strouse, G. F.; Younathan, J. N.; Baxter, S. M.; Meyer, T. J. *J. Am. Chem. Soc.* **1990**, *112*, 7571. (e) Strouse, G. F.; Worl, L. A.; Younathan, J. N.; Meyer, T. J. *J. Am. Chem. Soc.* **1989**, *111*, 9101.
(29) (a) Ryu, C. K.; Wang, R.; Schmehl, R. H.; Ferrere, S.; Ludwikow, M.; Merkert, J. W.; Headford, C. E. L.; Elliot, C. M. *J. Am. Chem. Soc.* **1992**, *114*, 430. (b) Yonemoto, E. H.; Riley, R. L.; Kim, Y. I.; Atherton, S. J.; Schmehl, R. H.; Mallouk, T. E. *J. Am. Chem. Soc.* **1992**, *114*, 8081. (c) Ryu, C. K.; Schmehl, R. H. *J. Phys. Chem.* **1989**, *93*, 7961.
(30) (a) Onho, T.; Nozaki, K.; Haga, M. *Inorg. Chem.* **1992**, *31*, 4256. (b) Nozaki, K.; Onho, T.; Haga, M. *J. Phys. Chem.* **1992**, *96*, 10880.
(31) Richter, M. M.; Brewer, K. J. *Inorg. Chem.* **1992**, *31*, 1594.
(32) Larson, S. L.; Cooley, L. F.; Elliot, C. M.; Kelley, D. F. *J. Am. Chem. Soc.* **1992**, *114*, 9504.
(33) Fujita, E.; Milder, S. J.; Brunschwig, B. S. *Inorg. Chem.* **1992**, *31*, 2079.
(34) (a) Bommarito, S. L.; Bretz, S. P.; Abruña, H. D. *Inorg. Chem.* **1992**, *32*, 194.
(35) Buranda, T.; Lei, Y.; Endicott, J. F. *J. Am. Chem. Soc.* **1992**, *114*, 6916.
(36) Ford, W. E.; Rodgers, M. A. J. *J. Phys. Chem.* **1992**, *96*, 2917.
(37) Downard, A. J.; Honey, G. E.; Phillips, L. F.; Steel, P. J. *Inorg. Chem.* **1992**, *30*, 2260.
(38) Furue, M.; Yoshidzumi, T.; Kinoshita, S.; Kushida, T.; Nozakura, S.; Kamachi, M. *Bull. Chem. Soc. Jpn.* **1991**, *64*, 1632.
(39) De Cola, L.; Barigelletti, F.; Balzani, V.; Hage, R.; Haasnoot, J. G.; Reedijk, J.; Vos, J. G. *Chem. Phys. Lett.* **1991**, *178*, 491.
(40) Murphy, W. R.; Brewer, K.; Gettliffe, G.; Petersen, J. D. *Inorg. Chem.* **1989**, *28*, 81.
(41) Fuchs, Y.; Lofters, S.; Dieter, T.; Shi, W.; Morgan, R.; Strekas, T. C.; Gafney, H. D.; Baker, A. D. *J. Am. Chem. Soc.* **1987**, *109*, 2691.
(42) Belser, P.; von Zelewsky, A.; Frank, M.; Seel, C.; Vögtle, F.; De Cola, L.; Barigelletti, F.; Balzani, V. *J. Am. Chem. Soc.*, in press.
(43) For preliminary results on energy transfer in **Ru^{II}·A·Os^{II}**, see: De Cola, L.; Barigelletti, F.; Balzani, V.; Belser, P.; von Zelewsky, A.; Frank, M.; Vögtle, F. *Mol. Cryst. Liq. Cryst.* in press.
(44) (a) Juris, A.; Balzani, V.; Belser, P.; von Zelewsky, A. *Helv. Chim. Acta* **1981**, *64*, 2175. (b) Sutin, N.; Creutz, C. *Adv. Chem. Ser.* **1978**, *168*, 1. (c) Lin, C. T.; Boettcher, W. J.; Chou, M.; Creutz, C.; Sutin, N. *J. Am. Chem. Soc.* **1976**, *98*, 6536.

^{1}H-NMR spectra were recorded on a Gemini 300 Varian spectrometer by using the proton impurities of the deuterated solvents as reference.

Fast atomic bombardment mass spectral data were obtained on a VG 7070 E spectrometer in a 3-nitrobenzyl alcohol matrix. Xe atoms were used for the bombardment (8 kV).

Absorption spectra were measured in acetonitrile solution at room temperature with a Perkin-Elmer Lambda 6 spectrophotometer. Luminescence experiments were performed in air-equilibrated acetonitrile solution at room temperature and in freshly distilled butyronitrile at 77 K. Luminescence spectra were obtained with a Perkin-Elmer LS 50 spectrofluorimeter. When necessary for comparison purposes, the luminescence intensity values were corrected to take into account the different absorbance values of the two solutions. Luminescence decay measurements were performed with an Edinburgh and an IBH single-photon counting equipment. Selection of excitation and emission wavelength was done by using monochromators and cut-off or band-pass optical filters. Analysis of the decay curves was performed by employing either home-made non-linear iterative programs or programs provided by the firms.

Flash photolysis experiments were carried out with a Nd:YAG laser (J. K. Lasers) with 20-ns pulse duration. The third harmonic (λ = 355 nm) with an energy of 8 mJ/pulse was used to excite the samples. The probe beam generated by a pulsed Xenon arc lamp crossed the irradiated area at right angle to the excitation. The light transmitted was focussed on the entrance slit of a monochromator and detected by an R936 Hamamatsu photomultiplier. Acquisition and processing of signals was obtained by a transient digitizer (Tektronix R7912) in conjunction with a PC.

Picosecond fluorescence lifetimes were detected with an apparatus based on a mode-locked, cavity-dumped Nd:YAG laser (Continuum PY62-10) and a streak camera (Hamamatsu C1587) equipped with a fast single sweep unit (M1952). The third harmonic (λ = 355 nm) with an energy of 6 mJ/pulse and a pulse duration of 35 ps was used to excite the samples. The light emitted was collected and fed into the entrance of a spectrograph (HR 250 Jobin-Yvon) and then focussed on the slit of the streak camera. Acquisition and processing of the streak images were performed via cooled CCD camera (Hamamatsu C3140) and related software running on a PC.

Typical images were the average of 250 + 5000 events. Data of emission intensity *vs* time over 20 nm around the maximum were averaged. The analysis of such profiles was performed with standard iterative nonlinear procedures. Time resolution of the system is 30 ps.

Photochemical experiments were performed in CH_2Cl_2 solution by using a mercury lamp and an interference filter with λ_{max} = 313 nm or with a tungsten lamp for irradiation in the visible region. The incident light intensity was measured by the ferrioxalate actinometer.[45]

Estimated errors are as follows: band maxima, ±2 nm; relative luminescence intensity ±2%; lifetimes, ±10%.

Preparation of the Bridging Ligand. 5-(Bromomethyl)-2,2′-bipyridine (**1**, Scheme I) has been synthesized according to Eaves et al.[46] Bicyclo-[2.2.2]octane-1,4-dicarboxaldehyde (**4**) has been synthesized according to Kumar et al.[47] The phosphonate ester **2** was readily obtained via an Arbuzov rearrangement. Ligand **5** can be prepared by a Wadsworth-Emmons reaction in 76% yield as pure all-(*E*) isomer (Scheme I). In contrast, the Witting olefination leads to lower yields and (*E*)/(*Z*) isomeric mixtures, containing the all-(*Z*) form (**6**) as the main product. To study the photoisomerization of the all-(*E*) isomer, we have also isolated a sample of pure all-(*Z*) isomer.

Diethyl 2,2′-bipyrid-5-ylmethylphosphonate (2). A 15.0-g (0.062-mol) sample of bromide **1** and 20.0 g (0.124 mol) triethyl phosphite were refluxed for 3 h. The mixture was evaporated to dryness; the residue was placed on a short silica-gel column and eluted with a mixture of CH_2Cl_2–methanol (10:1, v/v) to give a yellow oil. Yield: 17.7 g (96%). ^{1}H-NMR (200 MHz, $CDCl_3$): δ = 1.25 (t, 6H, CH_3), 3.15 (d, 2H, CH_2P), 4.05 (qd, 4H, OCH_2), 7.25 (ddd, 1H, bpy–H), 7.75 (td, 1H, bpy–H), 7.8 (dd, 1H, bpy–H), 8.34 (td, 1H, bpy–H), 8.35 (dd, 1H, bpy–H), 8.55 (dd, 1H, bpy–H), 8.65 (dm, 1H, bpy–H). ^{13}C-NMR (63 MHz, $CDCl_3$): δ = 16.4 (d, CH_3), 30.9 (d, $POCH_2$), 62.4 (d, $POCH_2$), 120.8 (d, CH), 121.1 (CH), 123.7 (CH), 128.0 (d, C_q), 136.9 (CH), 138.1 (d, CH), 149.2 (CH), 150.0 (d, CH), 154.9 (C_q), 155.4 (C_q). MS (EI, *m/z*): 306 (M^+, 25%), 170 ($M^+ - PO(OC_2H_5)_2$, 100%).

Scheme I

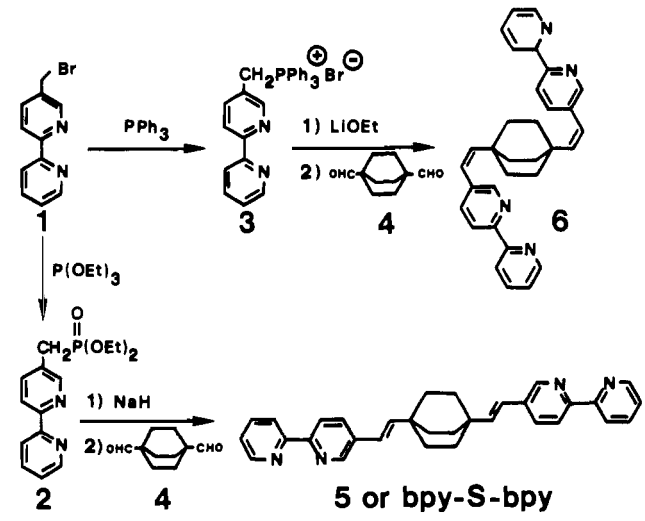

(2,2′-Bipyrid-5-ylmethyl)triphenylphosphonium Bromide (3). A solution of 3.0 g (12 mmol) of bromide **1** and 3.15 g (12 mmol) of triphenylphosphine were dissolved in 220 mL of dry xylene and refluxed for 3 h. The phosphonium salt precipitated out. After the mixture was allowed to stand for 12 h at room temperature, the white solid was filtered off and washed with *n*-hexane. Yield: 5.2 g (85%). Mp: 315–319 °C. ^{1}H-NMR (200 MHz, CD_3OD): δ = 5.15 (d, 2H, CH_2), 7.4–8.6 (m, 22H, Ar–H, bpy–H). MS (EI, *m/z*), 430 (M^+ – HBr, 100%), 262 (M^+ – HBr – $C_{11}H_8N_2$, 54%), 169 ($C_{11}H_9N_2^+$, 35%). Anal. Found (calcd for $C_{29}H_{24}BrN_2P$): C, 67.91 (68.11); N, 5.74 (5.48).

(*E*,*E*)-1,4-Bis[2-(2,2′-bipyridin-5-yl)ethenyl]bicyclo[2.2.2]octane (5; this bridging ligand will later be called bpy–S–bpy, as in Figure 1). Under argon atmosphere a solution containing 5.52 g (18 mmol) of phosphonate **2** in 50 mL of dry THF was added at room temperature to a suspension of 0.57 g (19 mmol) of sodium hydride (80% in an oil suspension) in 30 mL of dry THF. The mixture was stirred for 10 min. Then 1.36 g (8.2 mmol) of aldehyde **4** was dissolved in 50 mL of dry THF and added dropwise over a period of 1 h. Stirring was continued for 2 h, ice (200 g) was added, and a solid precipitated out. The crude product was filtered off and washed with water and *n*-hexane. For purification the residue was chromatographed on silica gel (eluent: $CHCl_3$–CH_3OH–aqueous ammonia, 300:10:1) and recrystallized from toluene. Yield: 2.9 g (76%). Mp: 310–312 °C. ^{1}H-NMR (200 MHz, $CDCl_3$): δ = 1.7 (s, 12H, CH_2), 6.3 (s, 4H, CH), 7.28 (ddd, 2H, bpy–H), 7.78 (td, 2H, bpy–H), 7.8 (td, 2H, bpy–H), 8.35 (m, 2H, bpy–H), 8.36 (m, 2H, bpy–H), 8.6 (d, 2H, bpy–H), 8.66 (dm, 2H, bpy–H). ^{13}C-NMR (63 MHz, $CDCl_3$): δ = 31.08 (CH_3), 34.17 (C_q), 121.25 (CH), 121.34 (CH), 121.89 (CH), 123.79 (C_q), 133.65 (CH), 133.94 (CH), 137.41 (CH), 142.96 (CH), 147.41 (CH), 149.01 (CH), 154.01 (C_q), 155.75 (C_q). MS (EI, *m/z*): 470 (M^+, 100%); found (calcd) for $C_{32}H_{30}N_4$, 470.2467 (470.2470). Anal. Found (calcd for $C_{32}H_{30}N_4$): C, 81.32 (81.67); H, 6.85 (6.42); N, 11.97 (11.9).

(*Z*,*Z*)-1,4-Bis[2-(2,2′-bipyridin-5-yl)ethenyl]bicyclo[2.2.2]octane (6). Under argon atmosphere 69 mg (10 mmol) of lithium wire was dissolved in 50 mL of dry methanol. Phosphonium salt **3** (2 g, 6.6 mmol) was added to the stirred solution. The mixture was cooled to 0 °C and treated dropwise with a solution of 500 mg of aldehyde **4** (3 mmol) in 50 mL of DMF. Stirring was continued for 1 h at 0 °C and for 2 h more at room temperature. The mixture was quenched with water; the solid was filtered off and washed with water, cold methanol, and *n*-hexane. The isomeric mixture was purified through fractioned recrystallization from toluene/*n*-hexane. The first crop contains 530 mg of pure all-(*Z*) isomer. Yield: 530 mg (38%). Mp: 158 °C. ^{1}H-NMR (400 MHz, $CDCl_3$): δ = 1.45 (s, 12H, CH_2), 5.5 (d, 2H, CH), 6.3 (d, 2H, CH), 7.25 (m, 2H, bpy–H), 7.55 (dd, 2H, bpy–H), 7.8 (td, 2H, bpy–H), 8.26 (d, 2H, bpy–H), 8.35 (d, 2H, bpy–H), 8.44 (d, 2H, bpy–H), 8.65 (dm, 2H, bpy–H). ^{13}C-NMR (63 MHz, $CDCl_3$): δ = 32.43 (CH_3), 34.57 (C_q), 120.0 (CH), 121.01 (CH), 123.61 (CH), 123.77 (CH), 135.26 (C_q), 136.96 (CH), 137.22 (CH), 143.84 (CH), 149.2 (CH), 149.22 (CH), 154.03 (C_q), 156.08 (C_q). MS (EI, *m/z*): 470 (M^+, 100%), found (calcd) for $C_{32}H_{30}N_4$: 470.2472 (470.2470). Anal. Found (calcd for $C_{32}H_{30}N_4$): C, 81.26 (81.67); H, 6.2 (6.42); N, 11.78 (11.9).

(45) Hatchard, C. G.; Parker, G. A. *Proc. R. Soc. London* **1956**, *A235*, 518.
(46) Eaves, J. G.; Munro, H. S.; Parker, D. *J. Chem. Soc., Chem. Commun.* **1985**, 684.
(47) Kumar, K.; Wang, S. S.; Sukenik, C. N. *J. Org. Chem.* **1984**, *49*, 665.

Table I. Absorption Maxima[a]

	λ, nm (ε, M^{-1} cm^{-1})			
Ru^{II}-A			451 (12 800)	288 (84 300)
Os^{II}-A	595 (2650)	481 (11 900)		290 (76 600)
Ru^{II}-A-Ru^{II}			451 (26 800)	288 (125 200)
Ru^{II}-A-Os^{II}	595 (3500)		451 (25 300)	290 (125 300)
Os^{II}-A-Os^{II}	595 (6100)	481 (25 600)		290 (124 900)
$Ru(bpy)_3^{2+}$ [b]			452 (14 600)	288 (76 600)
$Os(bpy)_3^{2+}$ [b]	579 (3270)	478 (11 100)	436 (10 700)	290 (78 000)

[a] Room temperature, acetonitrile solution. [b] Reference 22.

Preparation of the Metal Complexes. The metal complexes of the bridging ligand **5**, hereafter called bpy–S–bpy, were prepared according to the general one-step reaction

$$x[M(bpy)_2Cl_2] + \text{bpy–S–bpy} \xrightarrow[\text{excess } NH_4PF_6]{\uparrow\downarrow \text{methoxyethanol}} [(M(bpy)_2)_x(\text{bpy–S–bpy})](PF_6)_{2x}$$

$$x = 1, 2;\ M = Ru, Os$$

The mixed-metal $[(bpy)_2Ru(bpy–S–bpy)Os(bpy)_2](PF_6)_4$ compound was prepared in a two-step reaction. The monomeric $[(bpy)_2Os(bpy–S–bpy)](PF_6)_2$ species synthesized in the first step was reacted with a stoichiometric amount of $Ru(bpy)_2Cl_2$. Commercially available 2,2′-bipyridine and $RuCl_3·3H_2O$ were used as received. The precursors $Ru(bpy)_2Cl_2·2H_2O$[48] and $Os(bpy)_2Cl_2$[49] were prepared according to literature procedures. The solvents and reactants were of the highest purity commercially available and used as received.

$[(bpy)_2Ru(bpy–S–bpy)](PF_6)_2$ (Ru^{II}-A). A solution of 0.104 g (0.2 mmol) of $[Ru(bpy)_2Cl_2]·2H_2O$ dissolved in 35 mL of dichloromethane was carefully added dropwise over a period of 1 h to a hot solution (100 °C) of 0.094 g (0.2 mmol) of bpy–S–bpy in 15 mL of 2-methoxyethanol containing 5% H_2O. The mixture was refluxed for an additional 4 h. The solvents were evaporated, the metal complex was dissolved in water, and the solution was extracted twice with dichloromethane. A solution of 1.0 g of NH_4PF_6 dissolved in 5 mL of water was added to the aqueous part; the precipitate was filtered off and dried at 80 °C. The complex was purified first on an aluminum oxide column deactivated with 1.5% water (eluent, acetone–water (1.5%)) and then by recrystallization from an acetonitrile–diethyl ether mixture (vapor diffusion method), to give an orange solid (0.12 g, 51.2%). Anal. Found (calcd for $C_{52}H_{51}F_{15}N_8Na_{0.5}O_{2.5}P_{2.5}Ru$ including 2.5 mol of water and 0.5 mol of $NaPF_6$): C, 48.14 (48.36); H, 3.97 (3.98); N, 8.70 (8.68). FAB: m/z = 1030 (85%), $MH^+ - PF_6^-$; m/z = 884 (82%), $M^+ - 2PF_6^-$. ^{1}H-NMR (300 MHz, CD_3CN): δ = 1.53 (s, 12H, CH_2), 6.07–6.29 (m, 4H, CH), 7.34–8.5 (m, 30H, bpy– and (bpy–S–bpy)–H; these multiplets include the protons of the 2,2′-bipyridine ligands), 7.38 (dd, 4H, 5- and 5′-H), 7.70 (d, 4H, 6- and 6′-H), 8.04 (dd, 4H, 5- and 5′-H), 8.48 (d, 4H, 3- and 3′-H)). UV/vis: see Table I.

$[(bpy)_2Os(bpy–S–bpy)](PF_6)_2$ (Os^{II}-A). The preparation of this complex was performed with the same procedure as described above for the analogous Ru^{II} compound. A preparation on a 0.21-mmol scale with $[Os(bpy)_2Cl_2]$ gave 0.116 g (43.8%) of the dark olive complex. Anal. Found (calcd for $C_{52}H_{50}F_{18}N_8NaO_2OsP_3$ including 2 mol of water and 1 mol of $NaPF_6$): C, 43.25 (43.25); H, 3.52 (3.49); N, 7.75 (7.76). FAB: m/z = 1119 (100%), $MH^+ - PF_6^-$; m/z = 974 (72%), $M^+ - 2PF_6^-$. ^{1}H-NMR (300 MHz, CD_3CN): δ = 1.51 (s, 12H, CH_2), 6.02–6.32 (m, 4H, CH), 7.22–8.48 (m, 30H, bpy–and (bpy–S–bpy)–H; these multiplets include the protons of the 2,2′-bipyridine ligands), 7.29 (dd, 4H, 5- and 5′-H), 7.60 (d, 4H, 6- and 6′-H), 7.85 (dd, 4H, 5- and 5′-H), 8.47 (d, 4H, 3- and 3′-H)). UV/vis: see Table I.

$[(bpy)_2Ru(bpy–S–bpy)Ru(bpy)_2](PF_6)_4$ (Ru^{II}-A-Ru^{II}). A solution of 0.11 g (0.21 mmol) of $[Ru(bpy)_2Cl_2]·2H_2O$ and 0.05 g (0.106 mmol) of bpy–S–bpy in 20 mL of methoxyethanol–water (5%) was refluxed for 5 h. The solvents were evaporated and the complex purified as described before. Yield: 0.156 g (78.4%) of an orange solid. Anal. Found (calcd for $C_{72}H_{64}F_{24}N_{12}OP_4Ru_2$ including 1 mol of H_2O): C, 45.44 (45.63); H, 3.30 (3.40); N, 8.62 (8.87). FAB: m/z = 1730 (100%), $MH^+ - PF_6^-$; m/z = 1587 (80%), $M^+ - 2PF_6^-$. ^{1}H-NMR (300 MHz, CD_3CN): δ = 1.52 (s, 12H, CH_2), 6.03–6.32 (m, AB-system, 4H, CH), 7.31–8.51 (m, 46H, bpy– and (bpy–S–bpy)–H; these multiplets include the protons of the 2,2′-bipyridine ligands, 7.39 (dd, 4H, 5- and 5′-H), 7.69 (d, 4H, 6- and 6′-H), 8.04 (dd, 4H, 5- and 5′-H), 8.49 (d, 4H, 3- and 3′-H) and the two protons 6′ of the bpy–S–bpy ligand (7.52, s, 2H)). UV/vis: see Table I.

$[(bpy)_2Os(bpy–S–bpy)Os(bpy)_2](PF_6)_4$ (Os^{II}-A-Os^{II}). A solution of 0.732 g (0.128 mmol) of $[Os(bpy)_2Cl_2]$ and 0.03 g (0.064 mmol) of bpy–S–bpy in 20 mL methoxyethanol–water (5%) was refluxed for 8 h. The solvents were evaporated and the complex purified as described before. Yield: 0.074 g (56.2%) of dark olive solid. Anal. Found (calcd for $C_{74}H_{72}F_{24}N_{12}O_4P_4Os_2$ including 2 mol of H_2O and 1 mol of ethylene glycol): C, 41.47 (41.27); H, 3.23 (3.37); N, 7.69 (7.80). FAB: m/z = 1908 (60%), $M^+ - PF_6^-$; m/z = 1766 (100%), $M^+ - 2PF_6^-$. ^{1}H-NMR (300 MHz, CD_3CN): δ = 1.51 (s, 12H, CH_2), 6.02–6.31 (m, AB-system, 4H, CH), 7.23–8.48 (m, 46H, bpy–and (bpy–S–bpy)–H; these multiplets include the protons of the 2,2′-bipyridine ligands, 7.29 (dd, 4H, 5- and 5′-H), 7.59 (d, 4H, 6- and 6′-H), 7.85 (dd, 4H, 5- and 5′-H), 8.47 (d, 4H, 3- and 3′-H) and the two protons 6′ of the bpy–S–bpy ligand (7.44, s, 2H)). UV/vis: see Table I.

$[(bpy)_2Ru(bpy–S–bpy)Os(bpy)_2](PF_6)_4$ (Ru^{II}-A-Os^{II}). A solution of 0.05 g (0.0396 mmol) of $[(bpy)_2Os(bpy–S–bpy)](PF_6)_2$ and 0.0206 g (0.0396 mmol) of $[Ru(bpy)_2Cl_2]·2H_2O$ in 10 mL of methoxyethanol–water (5%) was refluxed for 4 h. The solvents were evaporated and the complex was purified as described before. Yield: 0.057 g (73.2%) of dark olive solid. Anal. Found (calcd for $C_{78}H_{78}F_{24}N_{12}O_3P_4OsRu$ including 1 mol of diethyl ether and 1 mol of ethylene glycol): C, 44.65 (44.56); H, 3.68 (3.74); N, 7.76 (7.99). FAB: m/z = 1821 (100%), $M^+ - PF_6^-$; m/z = 1677 (85%), $M^+ - 2PF_6^-$. ^{1}H-NMR (300 MHz, CD_3CN): δ = 1.51 (s, 12H, CH_2), 6.02–6.31 (m, two AB-systems, 4H, CH), 7.22–8.49 (m, 46H, bpy– and (bpy–S–bpy)–H; these multiplets include the protons of the 2,2′-bipyridine ligands, 7.29 (dd, 2H, 5- and 5′-H, Os side), 7.37 (dd, 2H, 5- and 5′-H, Ru side), 7.59 (d, 2H, 6- and 6′-H, Os side), 7.69 (d, 2H, 6- and 6′-H, Ru-side), 7.85 (dd, 2H, 5- and 5′-H, Os side), 8.04 (dd, 2H, 5- and 5′-H, Ru side), 8.48 (d, 4H, 3- and 3′-H) and the two protons 6′ of the bpy–S–bpy ligand (7.44, s, 1H, Os side, and 7.53, s, 1H, Ru side)). UV/vis: see Table I.

Oxidation with Ce(IV). The Os(II) complexes were oxidized in acetonitrile–water (10:1 v/v). This solvent was unsuitable for oxidation of the Ru(II) complexes because the Ru(III) species are stable only in very acid solution. Therefore a 40:60 acetonitrile–nitric acid (6%) v/v solvent was used for the Ru(II) complexes. In such a solvent the Os(II) species are oxidized in the dark. The solutions of the Ru(II) or Os(II) complexes (1.5×10^{-5} M) in the appropriate solvent were titrated with microliter aliquots of a 2.5×10^{-3} N Ce(IV) solution obtained from a 0.049 N standard solution of ammonium Ce(IV) nitrate in HNO_3 (6%) (Aldrich). The titration was performed by monitoring the change in absorbance in the visible region where the Ru(II) and Os(II) species exhibit intense absorption bands (Figure 2), whereas the absorbances of the Ru(III) and Os(III) species are very small.[50]

Results

Absorption Spectra and Photochemical Stability. The *E–E* form of the free bpy–S–bpy ligand (Figure 1) is insoluble in most solvents. In CH_2Cl_2 it exhibits a strong absorption band with maximum at 314 nm (ε = 54 200 M^{-1} cm^{-1}), accompanied by a less intense band with maximum at 268 nm (ε = 20 000 M^{-1} cm^{-1}). Both these bands are weaker and displaced to higher energy in the *Z–Z* form. Upon irradiation at 313 nm of a 1.5×10^{-5} M CH_2Cl_2 solution of the *E–E* form, spectral changes were observed with three clean isosbestic points, which indicate

(48) Sullivan, B. P.; Salmon, D. J.; Meyer, T. J. *Inorg. Chem.* **1978**, *17*, 3334.
(49) Lay, P. A.; Sargeson, A. M.; Taube, H. *Inorg. Synth.* **1986**, *24*, 291.
(50) Bryant, G. M.; Fergusson, J. E. *Aust. J. Chem.* **1971**, *24*, 275.

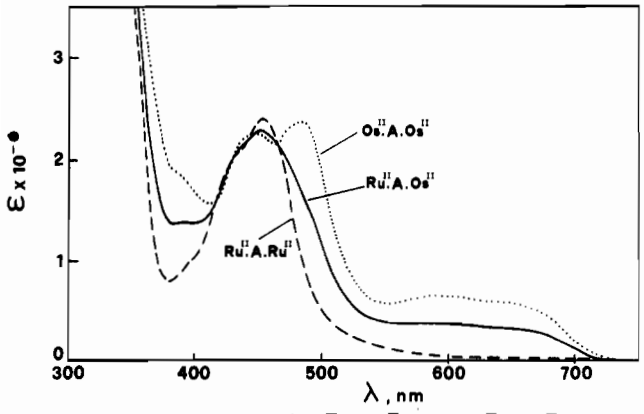

Figure 2. Absorption spectra of Ru^{II}·A·Ru^{II} (– –), Os^{II}·A·Os^{II} (···), and Ru^{II}·A·Os^{II} (—) in acetonitrile solution at room temperature.

photoisomerization to the *Z–Z* isomer. The quantum yield of the photoreaction is 0.12. Prolonged irradiation caused a photodecomposition of the *Z–Z* isomer.

The Ru^{II} and/or Os^{II} metal complexes were obtained by using the *E–E* form of the bridging ligand (Figure 1). They exhibit ligand-centered (LC) bands in the UV region accompanied by the characteristic[22] metal-to-ligand charge-transfer (MLCT) bands in the visible region (Table I). For illustration purposes, the spectra of the Ru^{II}·A·Ru^{II}, Os^{II}·A·Os^{II}, and Ru^{II}·A·Os^{II} species are shown in Figure 2. Irradiation of these metal complexes in CH_2Cl_2 under the same experimental conditions used for the free ligand did not cause any spectral change in the LC and in the MLCT bands, indicating that neither photoisomerization of the bridging ligand nor photodecomposition of the complexes takes place. Upon irradiation in the visible region, no photodecomposition was again observed in all cases, as for $[Ru(bpy)_3](PF_6)_2$.[51]

Luminescence. The bridging ligand bpy–S–bpy in its *E–E* form exhibits a fluorescence band with maximum at 360 nm in CH_2Cl_2 solution at room temperature. This band can no longer be observed in the metal complexes, including the monometallic species.

Regardless of the excitation wavelength, all the Ru^{II} and/or Os^{II} metal complexes exhibit the characteristic[22] MLCT luminescence both in rigid matrix at 77 K and in fluid solution at room temperature. For comparison purposes, luminescence experiments have also been performed on 1:1 mixtures of the dinuclear homometallic complexes. The results obtained have been gathered in Table II. Figure 3 compares the spectra of isoabsorptive (λ_{exc} = 464 nm) solutions of Ru^{II}·A·Os^{II} and of its homometallic parents Ru^{II}·A·Ru^{II} and Os^{II}·A·Os^{II}.

The procedure used to obtain values for the quenching of the luminescence of the Ru-based unit and the sensitization of the luminescence of the Os-based one in the Ru^{II}·A·Os^{II} mixed-metal compound (Table II) followed that previously described.[42] First, we have recorded the absorption spectra of equimolar (0.58×10^{-5} M) solutions of Ru^{II}·A·Ru^{II}, Os^{II}·A·Os^{II}, and Ru^{II}·A·Os^{II}, and we have found that they exhibit an isosbestic point at 464 nm (Figure 2). Then, equimolar solutions of Ru^{II}·A·Os^{II} and of a 1:1 mixture of Ru^{II}·A·Ru^{II} and Os^{II}·A·Os^{II} were prepared and were found to exhibit identical absorption spectra. The luminescence spectra of such solutions were recorded with excitation in the isosbestic point at 464 nm under identical instrumental conditions. The quenching of the Ru-based luminescence in the mixed-metal complex was obtained by comparing the heights of the emission bands at 625 nm where the luminescence of the Os-based unit is negligible (Figure 3). The results obtained showed that 91% of the luminescence intensity of the Ru-based component is quenched by the Os-based component. In order to elucidate the nature of the quenching mechanism, we have then compared the

(51) Durham, J.; Caspar, J. V.; Nagle, J. K.; Meyer, T. J. *J. Am. Chem. Soc.* **1982**, *104*, 4803.

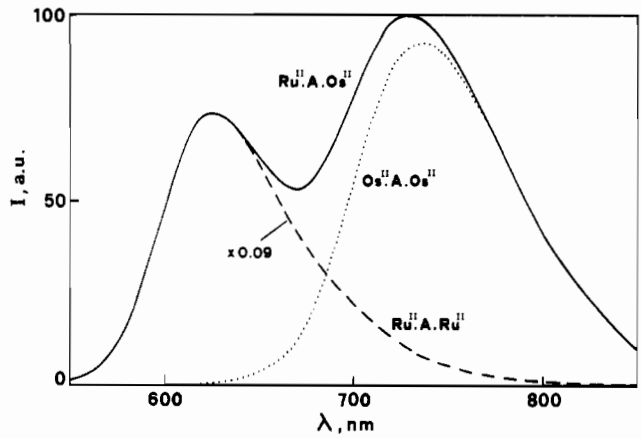

Figure 3. Luminescence spectra (acetonitrile solution, room temperature) of isoabsorptive (λ_{exc} = 464 nm) solutions of Ru^{II}·A·Os^{II} (—), Os^{II}·A·Os^{II} (···), and Ru^{II}·A·Ru^{II} (– –). The last spectrum has been normalized to the maximum of the Ru^{II}·A·Os^{II} spectrum.

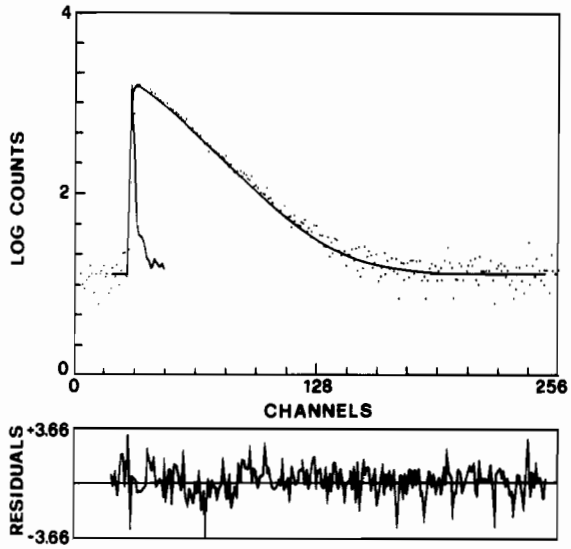

Figure 4. Rise and decay of the luminescence of the Os^{II}-based unit of Ru^{II}·A·Os^{II} (λ_{exc} = 337 nm; λ_{em} = 730 nm). Channel width: 1.92 ns/ch.

intensity of the Os-based luminescence (at 740 nm) in the mixed-metal complex with that of the Os^{II}·A·Os^{II} species, and we have found that, after correction for the tail of the residual Ru^{II}-based luminescence, they coincide within the experimental error (Figure 3).

The luminescence decay was strictly monoexponential for the mononuclear and homometallic binuclear species. For Ru^{II}·A·Os^{II}, the luminescence decay measured at 625 nm (Ru-based emission) was monoexponential (τ = 18 ns), whereas that measured at $\lambda > 665$ nm showed a biexponential decay (Figure 4) which was deconvoluted to yield a risetime τ_1 = 21 ns (in substantial agreement with the decay of the Ru-based emission), followed by a decay time τ_2 = 39 ns (equal to that of the Os^{II}·A and Os^{II}·A·Os^{II} species). The ratio of the preexponentials was $A_1/A_2 = -0.42$ (vide infra).

Electrochemical Behavior. The electrochemical potentials for the first oxidation and reduction processes of the various compounds are collected in Table III.

Generation of Mixed-Valence Compounds and Their Properties. It should be noticed that oxidation of the Os-based and Ru-based units was performed in solvents of different acid content (see Experimental Section) because of the instability of the Os^{II}-based units in the solvent used to oxidize the Ru^{II}-units and of the Ru^{III}-based units in the solvent used to oxidize the Os^{II}-based units. Addition of a standardized Ce(IV) solution (see Experimental Section) to a 1.5×10^{-5} M solution of Ru^{II}·A·Ru^{II},

Table II. Luminescence Data

	298 K[a]						77 K[b]			
	Ru			Os			Ru		Os	
	λ_{max}, nm	τ, ns	I_{rel}[c]	λ_{max}, nm	τ, ns	I_{rel}[c]	λ, nm	τ μs	λ nm	τ μs
Ru^{II}·A	625	205	50				599	4.54		
Os^{II}·A				736	40	50			723	0.97
Ru^{II}·A·Ru^{II}	628	209	100				604	4.46		
Os^{II}·A·Os^{II}				740	40	100			727	0.89
$^1/_2Ru^{II}$·A·Ru^{II} + $^1/_2Os^{II}$·A·Os^{II}	628	205	50	*d*	*d*	*d*	600			
Ru^{II}·A·Os^{II}	625	18[e]	4.5	740[f]	39	50[f]	601	0.031	723	1.0
$Ru(bpy)_3^{2+}$	615	170	52[g]				582	5.0		
$Os(bpy)_3^{2+}$				743	49				710	0.83

[a] Air-equilibrated acetonitrile solution. [b] Butyronitrile solution. [c] Excitation was performed at 464 nm, which is an isosbestic point between the Ru-based and Os-based units on equimolar solutions; for comparison purposes, the luminescence intensities of Ru^{II}·A·Ru^{II} at 628 nm and Os^{II}·A·Os^{II} at 740 nm were taken as 100. [d] The Os-based emission is covered by the tail of the stronger Ru-based emission. [e] To be compared with the risetime of the Os-based emission (21 ns). [f] After correction for the residual Ru-based emission (Figure 4). [g] The luminescence quantum yield under these conditions is 0.016.[22]

Table III. Electrochemical Data[a]

	redox potentials, V [rel current intens] (peak separation $E_a - E_c$, mV)		
	oxidn		
	Ru	Os	redn[b]
Ru^{II}·A	+1.25 [1] (110)		−1.31 [1] (80)
Os^{II}·A		+0.81 [1] (75)	−1.25 [1] (85)
Ru^{II}·A·Ru^{II}	+1.25 [2] (135)		−1.31 [2] (90)
Os^{II}·A·Os^{II}		+0.81 [2] (95)	−1.25 [2] (90)
Ru^{II}·A·Os^{II}	+1.25 [1] (90)	+0.81 [1] (75)	−1.30 [2] (120)
$Ru(bpy)_3^{2+}$	+1.26 [1] (95)		−1.35 [1] (90)
$Os(bpy)_3^{2+}$ [c]		+0.83 [1] (80)	−1.28 [1] (80)

[a] Acetonitrile solution, room temperature; potential values *vs* SCE. [b] The second and third reduction peaks are irreversible. [c] Reference 22b.

Os^{II}·A·Os^{II}, and Ru^{II}·A·Os^{II} caused strong changes in the absorption spectra, fully comparable to those obtained for oxidation of $Ru(bpy)_3^{2+}$ and $Os(bpy)_3^{2+}$. It is well-known, in fact, that $Ru(bpy)_3^{3+}$ and $Os(bpy)_3^{3+}$ show in the visible region an absorption band with λ_{max} = 676 and 563 nm, respectively, with small molar absorption coefficient (409 and 585 M^{-1} cm^{-1}, respectively).[50] These bands are assigned to doublet → doublet ligand-to-metal charge transfer (LMCT) transitions from a π orbital of the ligands to the t_{2g} (in octahedral symmetry) metal orbitals, which have an empty place because of the d^5 electronic configuration of Ru(III) and Os(III).

For the two homometallic compounds, the absorbance at 450 nm (Ru^{II}·A·Ru^{II}) and that at 630 nm (Os^{II}·A·Os^{II}) decreased linearly with increasing number of added oxidation equivalents and disappeared after addition of 2 equiv of oxidant. For Ru^{II}·A·Os^{II}, addition of 1 equiv of oxidant caused the disappearance of the Os-based absorption, as expected because of the different oxidation potentials of the Os-based and Ru-based moieties (Table III). For this species, if allowance is made for the changes due to the oxidation of the Os-based moiety, the Ru-based absorbance at 450 nm remains unchanged after addition of 1 equiv of oxidant.

Oxidation of the dimetallic species caused a decrease in the luminescence intensity. Such a decrease is linear for both the Os-based and Ru-based luminescence of the Ru^{II}·A·Os^{II} species; after addition of 1 equiv of oxidant, the Os-based luminescence is completely quenched, whereas a weak Ru-based luminescence, with a lifetime of 115 ps, is still present. Flash photolysis experiments showed that the quenching of the Ru-based luminescent excited state in $*Ru^{II}$·A·Os^{III} leads to a transient species which exhibits the absorption spectrum shown in Figure 5. Comparison with the spectra of Figure 1 clearly shows that this transient is the Ru^{III}·A·Os^{II} species, which decays to Ru^{II}·A·Os^{III} with a rate constant of 1.0×10^6 s^{-1} (Figure 5, inset).

For the Ru^{II}·A·Ru^{II} and Os^{II}·A·Os^{II} species, the decrease in the luminescence intensity upon addition of the oxidant is not linear (Figure 6). Luminescence lifetimes measured after addition of 1.2 equiv of oxidant gave a biexponential decay with lifetimes

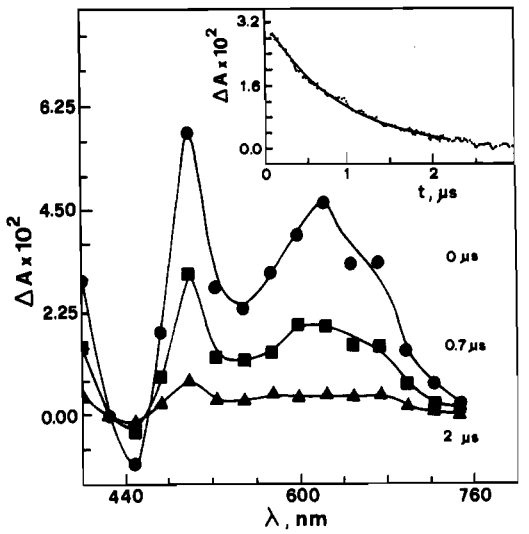

Figure 5. Transient absorption spectra upon excitation (λ = 355 nm) of Ru^{II}·A·Os^{III}. The inset shows the decay of the transient absorbance measured at 650 nm.

209 ns and 940 ps for Ru^{II}·A·Ru^{II}, and 40 ns and 200 ps for Os^{II}·A·Os^{II}.

For all the mixed-valence species, absorption measurements up to 1400 nm excluded the presence of intervalence transfer bands with $\epsilon > 50$ M^{-1} cm^{-1}.

Discussion

Properties of the Compounds and Intercomponent Interactions. Extensive investigations on mononuclear Ru(II) and Os(II) complexes[22] have shown that (i) oxidation is metal centered, (ii) Os(II) is easier to oxidize than Ru(II), (iii) reduction is ligand centered, (iv) the absorption bands in the visible region are due to spin-allowed metal-to-ligand charge-transfer (MLCT) tran-

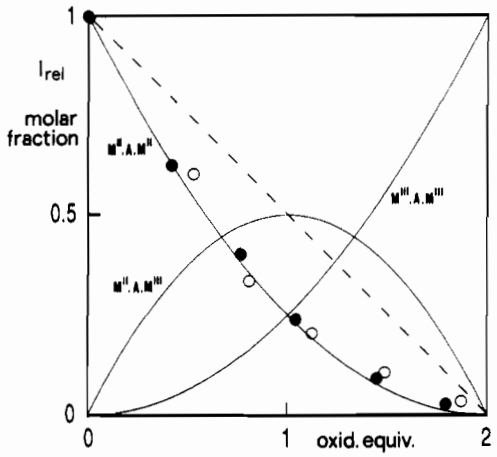

Figure 6. Changes in the relative luminescence intensities of Ru^{II}·A·Ru^{II} (○, 620 nm) and Os^{II}·A·Os^{II} (●, 730 nm) upon oxidation. The curves represent the molar fractions of the M^{II}·A·M^{II}, M^{II}·A·M^{III}, and M^{III}·A·M^{III} species, as a function of added oxidation equivalents. The dotted straight line shows the expected behavior of the luminescence intensity of a M^{II}·A·M^{II} system where oxidation of one metal-based unit does not affect the luminescence of the other moiety. For more details, see text.

sitions (and related spin-forbidden transitions for Os(II) complexes), (v) luminescence takes place from the lowest-energy excited state, which formally is a triplet MLCT level, and (vi) the luminescent excited state is very rapidly populated with unitary efficiency regardless of the excitation wavelength.

Each metal-containing unit of the compounds investigated in this work can be viewed as a mixed-ligand complex since the coordination sites of the bridging ligands have properties slightly different from those of bpy because of the presence of a substituent (S) in the 5-position (Figure 1). Comparison of the spectroscopic and electrochemical properties of Ru^{II}·A and Os^{II}·A with those of $Ru(bpy)_3^{2+}$ and $Os(bpy)_3^{2+}$ (Tables I–III) shows that the effect of the substituent S in the 5-position is very small. The strongest (but still quite small) difference can be found, as expected, in the first (ligand-centered) reduction potential, which is about 30–40 mV more positive for Ru^{II}·A and Os^{II}·A compared with that for $Ru(bpy)_3^{2+}$ and $Os(bpy)_3^{2+}$, respectively.

Spacer S of the bpy–S–bpy bridging ligand (Figure 1) is 9 Å long. It is made of a rigid bicyclooctane component linked to two ethylene-type units, each of which exhibits an *E* geometrical configuration. When bpy–S–bpy is linked to one or two metal units, no thermal or photochemical isomerization takes place. Although rotation about the single C–C bonds which connect the ethylene units to the bpy ligands and to the central bicyclooctane component can occur, in the binuclear compounds the distance between the metal centers, which are separated by 15 bonds, is confined to 17 ± 1 Å.

In oligonuclear complexes electronic interaction between the mononuclear components may range from very strong (with profound changes in the spectroscopic and electrochemical properties on passing from mononuclear to oligonuclear species) to very weak (with almost equal properties for separated and bridged units) depending on the type of bridge.

An important point to notice is that the first oxidation potential, the first reduction potential, the absorption maxima, and all the luminescence properties are identical (within the experimental errors) for Ru^{II}·A and Ru^{II}·A·Ru^{II} and for Os^{II}·A and Os^{II}·A·Os^{II}. This suggests little or no electronic interaction between the identical metal-containing components that are present in the dinuclear homometallic compounds. Further evidence of a very weak interaction (if any) comes from (a) the identical oxidation potentials of the Os-based moieties in Os^{II}·A·Os^{II} and Ru^{II}·A·Os^{II} and of the Ru-based moieties in Ru^{II}·A·Ru^{II} and Ru^{II}·A·Os^{II} and (b) the identical absorption spectra exhibited by the mixed-metal Ru^{II}·A·Os^{II} complex and the 1:1 mixture of its homometallic

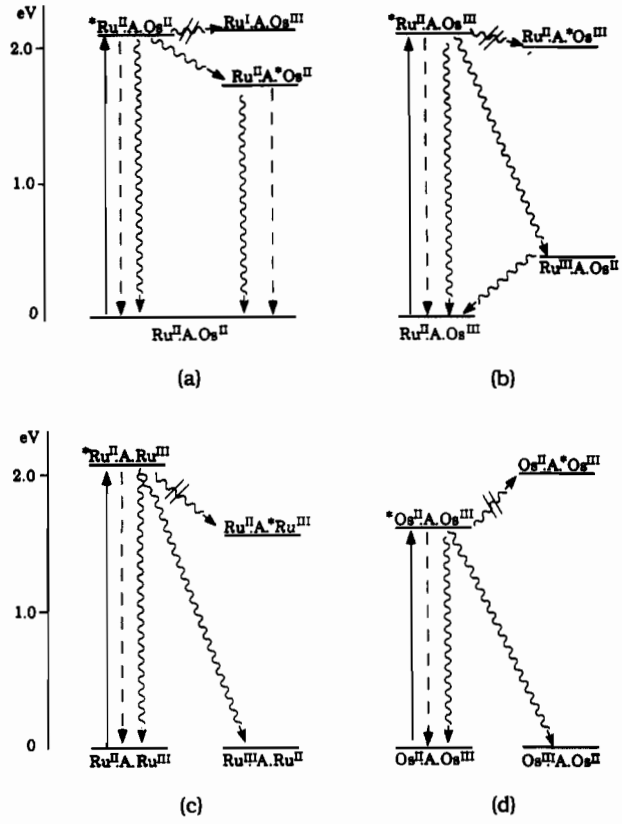

Figure 7. Energy level diagrams showing the photoinduced energy and electron transfer deactivation processes in Ru^{II}·A·Os^{II} (a), Ru^{II}·A·Os^{III} (b), Ru^{II}·A·Ru^{III} (c), and Os^{II}·A·Os^{III} (d). Key: full line, excitation; dotted line, luminescence; wavy line, radiationless decay. For more details, see text.

"parent" complexes Ru^{II}·A·Ru^{II} and Os^{II}·A·Os^{II}. The absence of intense ($\epsilon > 50$ M^{-1} cm^{-1}) intervalence transfer bands in the mixed-valence compounds confirms the lack of strong intercomponent interaction. It should be recalled, however, that even an interaction of a few reciprocal centimeters (which cannot be noticed in spectroscopic and electrochemical experiments) is sufficient to cause fast intercomponent energy- and electron-transfer processes.[5]

In the dinuclear compounds light is independently absorbed by the Ru(II)- and Os(II)-based units. In each chromophoric unit rapid deactivation of the excited state reached by light absorption leads to the population of the lowest energy, long-lived, luminescent excited state.[22] The Ru(III)- and Os(III)-based units do not exhibit any long-lived and luminescent level.[50]

Intercomponent Energy Transfer in Ru^{II}·A·Os^{II}. The Ru-based luminescence intensity of a 1:1 mixture of Ru^{II}·A·Ru^{II} and Os^{II}·A·Os^{II} in acetonitrile solution at room temperature is 50% that of an isoabsorptive (at the 464-nm isosbestic point, Figure 2) Ru^{II}·A·Ru^{II} solution, indicating that *intermolecular* quenching does not occur under the experimental conditions used (lifetime of the Ru^{II}·A·Ru^{II} excited state, 209 ns; Os^{II}·A·Os^{II} concentration, 1.0×10^{-5} M). However, the luminescence intensity of the Ru-based unit of Ru^{II}·A·Os^{II} is 9% that of an equimolar 1:1 mixture of Ru^{II}·A·Ru^{II} and Os^{II}·A·Os^{II} (Table II). This shows that in Ru^{II}·A·Os^{II} the luminescence of the Ru-based unit is *intramolecularly* quenched by the Os-based unit.

In principle, the quenching can be due to electron- (el tr) or energy-transfer (en tr) processes (Figure 7a). From the excited state energy of the Ru-based unit (2.06 eV)[52] and the redox

(52) Excited state energies have been estimated as the energy of the emission maximum at 77 K. Other methods give more refined but practically equivalent results.

potentials shown in Table III, it can be estimated[53] that the reductive quenching process

$$*Ru^{II}\cdot A\cdot Os^{II} \xrightarrow{\text{el tr (redn)}} Ru^{I}\cdot A\cdot Os^{III} \quad (1)$$

would be slightly endoergonic (+0.05 eV) and that the oxidative quenching process

$$*Ru^{II}\cdot A\cdot Os^{II} \xrightarrow{\text{el tr (ox)}} Ru^{III}\cdot A\cdot Os^{I} \quad (2)$$

would be strongly endoergonic (+0.49 eV). Therefore quenching by electron transfer, which implies a large reorganization energy in polar solvents (vide infra), is unlikely. By contrast, quenching via energy transfer

$$*Ru^{II}\cdot A\cdot Os^{II} \xrightarrow{\text{en tr}} Ru^{II}\cdot A\cdot *Os^{II} \quad (3)$$

is exoergonic (–0.35 eV). Evidence for energy transfer as the sole quenching mechanism was obtained from a comparison between the corrected luminescence intensities of $Ru^{II}\cdot A\cdot Os^{II}$ and $Os^{II}\cdot A\cdot Os^{II}$, which showed that the quenching of the luminescence of the Ru-based unit is accompanied *quantitatively* by the sensitization of the luminescence of the Os-based unit.

As one can see from Table II, the quenching of the luminescence intensity of the Ru-based component is accompanied by a parallel quenching of the excited-state lifetime. Furthermore, the decay of the Ru-based excited state is accompanied by the rise of the Os-based excited state.[54] The rate constant for energy transfer can be calculated from

$$k_{en} = \frac{1}{\tau} - \frac{1}{\tau^{\circ}} \quad (4)$$

where τ and τ° are the luminescence lifetimes of the Ru-based component in $Ru^{II}\cdot A\cdot Os^{II}$ and in the $Ru^{II}\cdot A\cdot Ru^{II}$ model compound, respectively. From the lifetime values shown in Table II, k_{en} results to be 5.0×10^7 s^{-1}. A very similar value (4.7×10^7 s^{-1}) is obtained if k_{en} is calculated from

$$k_{en} = \frac{1}{\tau^{\circ}}\left(\frac{I^{\circ}}{I}\right) \quad (5)$$

where I and I° are the relative luminescence intensities of isoabsorptive solutions (λ = 464 nm) of $Ru^{II}\cdot A\cdot Os^{II}$ and of a 1:1 mixture of $Ru^{II}\cdot A\cdot Ru^{II}$ and $Os^{II}\cdot A\cdot Os^{II}$, respectively.

Intercomponent Luminescence Quenching in Mixed-Valence Compounds. Partial oxidation of the $Ru^{II}\cdot A\cdot Ru^{II}$, $Os^{II}\cdot A\cdot Os^{II}$, and $Ru^{II}\cdot A\cdot Os^{II}$ compounds leads to the $Ru^{II}\cdot A\cdot Ru^{III}$, $Os^{II}\cdot A\cdot Os^{III}$, and $Ru^{II}\cdot A\cdot Os^{III}$ mixed-valence species where the nonluminescent oxidized unit can quench the luminescence of the nonoxidized unit.

In the case of $Ru^{II}\cdot A\cdot Os^{II}$, the two metal ions have substantially different oxidation potentials (Table III) and do not interact appreciably (*vide supra*). Therefore selective oxidation of the Os-based unit can be achieved. The luminescence from this unit (λ_{em} = 730 nm) decreases linearly on addition of the oxidant (which converts the emissive Os^{II}-based unit into the nonabsorbing and nonemissive Os^{III}-based one) and, as expected, disappears after the addition of 1 equiv of oxidant. A linear decrease of the Ru-based (λ_{em} = 625 nm) luminescence intensity also occurs, but this luminescence signal does not disappear after the oxidation of the Os-based unit. The intensity of the residual luminescence is <1.5% that of $Ru^{II}\cdot A\cdot Ru^{II}$ and exhibits a lifetime of 115 ps. These results show that in $Ru^{II}\cdot A\cdot Os^{III}$ the luminescent Ru-based excited state is quenched by the Os^{III}-based component with a rate constant of 8.7×10^9 s^{-1}. The energy level diagram schematized in Figure 7b shows that the quenching of the $*Ru^{II}\cdot A\cdot Os^{III}$ luminescent excited state can take place (i) by intercomponent energy transfer to form the $Ru^{II}\cdot A*Os^{III}$ species (where the Os^{III}-based excited state is LMCT in nature[55]), which will then relax to the ground state, or (ii) by intercomponent electron transfer via the intervalence-transfer excited state $Ru^{III}\cdot A\cdot Os^{II}$. The energy-transfer rate constant for $*Ru^{II}\cdot A\cdot Os^{III}$ should be comparable to the energy-transfer rate constant for $*Ru^{II}\cdot A\cdot Os^{II}$, 5.0×10^7 (*vide infra*). Therefore the energy-transfer pathway cannot account for the observed quenching rate constant (8.7×10^9 s^{-1}), which is more than 200 times larger than that found for $*Ru^{II}\cdot A\cdot Os^{II}$. Laser flash photolysis, in fact, shows that the quenching takes place by electron transfer, leading to the $Ru^{III}\cdot A\cdot Os^{II}$ isomer which then decays to its intervalence ground-state isomer $Ru^{II}\cdot A\cdot Os^{III}$ with a rate constant of 1.0×10^6 s^{-1} (Figure 5).

In the case of $Ru^{II}\cdot A\cdot Ru^{II}$ and $Os^{II}\cdot A\cdot Os^{II}$, the behavior upon oxidation is more complicated because the two metal units in each supramolecular species are oxidized at the same potential (Table III). Therefore addition of the oxidant leads to a statistical distribution of the $M^{II}\cdot A\cdot M^{II}$, $M^{II}\cdot A\cdot M^{III}$, and $M^{III}\cdot A\cdot M^{III}$ species, as represented in Figure 6.[56] Oxidation causes a linear decrease of absorbance since each equivalent of oxidant transforms an equivalent of strongly absorbing M(II)-based unit into a weakly absorbing M(III)-based unit.[50] The luminescence behavior, however, is different. As one can see from Figure 6, the values of the luminescence intensity lie *below* the dotted straight line that represents the behavior expected for isolated luminescent M(II)-based units, and follow (within the experimental error) the curve which represents the fraction of $M^{II}\cdot A\cdot M^{II}$ species. This shows that there is a quenching effect of the M(III)-based component on the luminescent M(II)-based one in the $M^{II}\cdot A\cdot M^{III}$ species. Although the scattering of the experimental data is large (especially in the case of the $Ru^{II}\cdot A\cdot Ru^{II}$ system, whose oxidized form is rather unstable), we can conclude that the efficiency of intercomponent quenching in the $*M^{II}\cdot A\cdot M^{III}$ species is certainly larger than 90%. Lifetime measurements carried out on solution containing 1.2 oxidation equiv (i.e., where 60% of the M^{II}-based units were oxidized) showed a biexponential decay. The longer component (209 and 40 ns for the $Ru^{II}\cdot A\cdot Ru^{II}$ and $Os^{II}\cdot A\cdot Os^{II}$ systems, respectively) can be assigned to the excited-state decay in the residual $M^{II}\cdot A\cdot M^{II}$ species. The shorter component (940 and 200 ps respectively) can be assigned to the decay of the M(II)-based luminescent excited state in the $M^{II}\cdot A\cdot M^{III}$ species. From these data, the intercomponent quenching constants result to be 1.1×10^9 s^{-1} for $*Ru^{II}\cdot A\cdot Ru^{III}$ and 5.0×10^9 s^{-1} for $*Os^{II}\cdot A\cdot Os^{III}$.

In the case of $*Ru^{II}\cdot A\cdot Ru^{III}$ (Figure 7c), two quenching paths are available. The energy-transfer path cannot be faster than that found in $*Ru^{II}\cdot A\cdot Os^{II}$ (5.0×10^7 s^{-1}) because the two processes have a comparable electronic factor and that in $*Ru^{II}\cdot A\cdot Ru^{III}$ has a less favorable nuclear factor (inverted region, *vide infra*). Therefore this path cannot account for the relatively large quenching rate constant (1.1×10^9 s^{-1}) experimentally observed. We conclude that the intercomponent quenching is due to electron transfer, which is strongly exoergonic (2.06 eV; for more details, see next section).

For $*Os^{II}\cdot A\cdot Os^{III}$ (Figure 7d), energy transfer is endoergonic (~0.3 eV), and the observed intercomponent quenching can only be attributed to the strongly exoergonic (1.71 eV) electron-transfer process.

(53) Balzani, V.; Bolletta, F.; Gandolfi, M. T.; Maestri M. *Top. Curr. Chem.* **1978**, *75*, 1.

(54) Since selective excitation of the Ru-based chromophoric unit cannot be obtained, a substantial fraction of Os-based excited states are already present when the Os-based excited states originating from the energy transfer process begin to accumulate (λ_{exc} = 337 nm). This is reflected in the value of the ratio between the coefficients, $A_1/A_2 = -0.42$ (see Results); a value of –1 for this ratio is expected for selective excitation of the donor.

(55) Os(III) is a less powerful oxidant than Ru(III); therefore the LMCT transitions lie at higher energy in the Os(III) compound. The maximum of the lowest energy absorption band is at 1.83 and 2.2 eV for the Ru(III) and Os(III) compounds, respectively.[50] The zero–zero transition is expected to be 0.2–0.3 eV lower in energy.

(56) The fractions of the three species are given by $(1-x)^2$, $2(1-x)x$, and x^2, where x is the fraction of added oxidation equivalents.

In conclusion, the excited state quenching in $*Ru^{II}$·A·Os^{III}, $*Ru^{II}$·A·Ru^{III}, and $*Os^{II}$·A·Os^{III} is due to intercomponent electron transfer in all cases.

Rate Constants of the Energy and Electron-Transfer Processes. In the $*Ru^{II}$·A·Os^{II} species (Figure 7a) an energy transfer process, which leads to the population of the Ru^{II}·A·$*Os^{II}$ excited state, takes place with rate constant 5.0×10^7 s^{-1}. Intermolecular energy transfer from $*Ru(bpy)_3^{2+}$ to $Os(bpy)_3^{2+}$ in water is almost diffusion controlled ($k = 1.9 \times 10^9$ M^{-1} s^{-1})[57] indicating that the order of magnitude of the energy-transfer rate constant in the encounter complex is larger than 1×10^9 s^{-1}. The small value found for the rate constant of the intercomponent energy-transfer process in $*Ru^{II}$·A·Os^{II} must be due to the separation imposed by the rigid bridging ligand (Figure 1). In fact, the through-space center-to-center distance in the dinuclear complexes, r, is 17 Å, and the two metal centers are separated by 15 bonds.

Electronic energy transfer processes can occur by two mechanisms:[5] the Förster-type mechanism,[58] based on coulombic interactions, and the Dexter-type mechanism,[59] based on exchange interactions. The Förster-type mechanism is a long-range mechanism (its rate falls off as r^6), which is efficient when the radiative transitions corresponding to the deactivation and the excitation of the two partners have high oscillator strength. The Dexter-type mechanism is a short-range mechanism (its rate falls off as e^r) that requires orbital overlap between donor and acceptor. When the donor and acceptor are linked together by chemical bonds, the exchange interaction can be enhanced (superexchange mechanism[17,60]). The energy transfer processes that take place in systems similar to Ru^{II}·A·Os^{II}, but involve flexible bridges,[29c,38,61,62] have been interpreted as occurring via a Förster-type mechanism or both Förster- and Dexter-type mechanisms.[63]

The expected rate of energy transfer according to the Förster mechanism can be calculated on the basis of spectroscopic quantities by

$$k_{en} = 5.87 \times 10^{-25}(\Phi_D/n^4\tau_D r^6)\int_0^\infty F_D(\bar{\nu})\epsilon_A(\bar{\nu})\,d\bar{\nu}/\bar{\nu}^4 \qquad (6)$$

For Ru^{II}·A·Os^{II}, $\Phi_D = 0.014$, $\tau_D = 209$ ns, $r = 17$ Å, and the value of the overlap integral is 4.3×10^{-14} M^{-1} cm^3. The value obtained for k_{en} from eq 6 (2.1×10^7 s^{-1}) is of the same order of magnitude of the experimental value (5.0×10^7 s^{-1}). In view of the approximations involved, it could well be that the Förster mechanism accounts for the observed energy-transfer process. The possibility cannot be excluded, however, that a Dexter-type energy-transfer mechanism is also involved and plays a major role.

The rate constant for a Dexter-type (electron-exchange) energy transfer may be expressed in an absolute rate formalism[64,65] as

$$k_{en} = \nu_N \kappa \exp(-\Delta G^*_{en}/RT) \qquad (7)$$

where ν_N is the average nuclear frequency factor, κ is the electronic transmission coefficient, and ΔG^*_{en} is the free activation energy. This last term can be expressed by the Marcus quadratic relationship[66]

$$\Delta G^*_{en} = \left(\frac{\lambda_{en}}{4}\right)\left(1 + \frac{\Delta G^\circ_{en}}{\lambda_{en}}\right)^2 \qquad (8)$$

where λ_{en} is the intrinsic barrier and ΔG°_{en} the standard free energy change of the energy transfer process. Using the reasonable assumptions[29c,64,65,67] that (i) the free energy change can be expressed by the difference between the zero–zero spectroscopic energies of the donor and acceptor excited state (–0.35 eV), and (ii) the λ_{en} parameter is equal to the spectroscopic Stokes shift (i.e., about 0.2 eV)[25,67] between absorption and emission of donor (which is approximately equal to that of the acceptor), the process falls in the Marcus inverted region with a value of ~0.28 for the exponential term of eq 7 at room temperature. Assuming $\nu_N = 1 \times 10^{13}$ s^{-1}, the experimental value $k_{en} = 5.0 \times 10^7$ s^{-1} yields (eq 4) a value of $\sim 2 \times 10^{-5}$ for the electronic factor κ. This shows that the process is strongly nonadiabatic. In the nonadiabatic limit,[5,14] eq 7 can be written as

$$k_{en} = \nu_{en} \exp(-\Delta G^*_{en}/RT) \qquad (9)$$

where ν_{en} is an electronic frequency given by

$$\nu_{en} = \frac{2(H_{en})^2}{h}\left(\frac{\pi^3}{\lambda_{en}RT}\right)^{1/2} \qquad (10)$$

where H_{en} is the electronic matrix element. Since $\nu_{en} \sim 1.8 \times 10^8$ s^{-1} and $\lambda_{en} = 0.2$ eV, H_{en} can be estimated to be ~0.6 cm^{-1} by the assumption of an exchange mechanism.

For $*Ru^{II}$·A·Os^{III}, $*Ru^{II}$·A·Ru^{III}, and $*Os^{II}$·A·Os^{III} (Figure 7b–d), deactivation takes place only by electron transfer. This conclusion is straightforward in the case of $*Os^{II}$·A·Os^{III}, since electron transfer is the only viable (i.e., exoergonic) deactivation process. For $*Ru^{II}$·A·Os^{III}, an electron-transfer quenching mechanism is supported by the fact that the Ru^{III}·A·Os^{II} electron-transfer product was observed. On the other hand, the rate of energy-transfer processes in $*Ru^{II}$·A·Os^{III} and $*Ru^{II}$·A·Ru^{III} via an exchange mechanism[68] can be estimated by eqs 8 and 9, taking the same electronic factor and intrinsic barrier as for the $*Ru^{II}$·A·Os^{II} system and an exoergonicity of 0.15 eV for $*Ru^{II}$·A·Os^{III} and 0.5 eV for $*Ru^{II}$·A·Ru^{III}. The results obtained ($k_{en} = 1.6 \times 10^8$ for $*Ru^{II}$·A·Os^{II} $k_{en} = 2 \times 10^6$ s^{-1} for $*Ru^{II}$·A·Ru^{III}) show that energy transfer cannot account for the observed quenching constants (8.7×10^9 and 1.1×10^9 s^{-1}, respectively).

The electron transfer processes taking place in $*Ru^{II}$·A·Os^{III}, $*Ru^{II}$·A·Ru^{III}, and $*Os^{II}$·A·Os^{III} are characterized by a different exoergonicity (1.62, 2.06, and 1.71 eV, respectively). The electronic interaction energy is likely to be very small and very similar for the three processes, since in each case a π^* electron localized on a bpy ligand of the M^{II}-based excited unit is tranferred to a t_{2g} orbital of the oxidized metal of the other unit. The reorganizational barrier to electron transfer should also be the same in each case, since each process implies an electron transfer from a 2+ excited state to a 3+ ground state. Therefore, these three processes constitute a homogeneous family.

According to current theories,[5,7,14] the rate of an electron-transfer process in the nonadiabatic limit can be expressed by

$$k_{el} = \nu_{el} \exp(-\Delta G^*_{el}/RT) \qquad (11)$$

(57) Creutz, C.; Chou, M.; Netzel, T. L.; Okamura, M.; Sutin, N.; *J. Am. Chem. Soc.* **1980**, *102*, 1309.
(58) Förster, Th. H. *Discuss. Faraday Soc.* **1959**, *27*, 7.
(59) Dexter, D. L. *J. Chem. Phys.* **1953**, *21*, 836.
(60) McConnell, H. M. *J. Chem. Phys.* **1961**, *35*, 508.
(61) Schmehl, R. H.; Auerbach, R. A.; Walcholtz, W. F.; Elliott, C. M.; Freitag, R. A. *Inorg. Chem.* **1986**, *25*, 2440.
(62) Schmehl, R. H.; Auerbach, R. A.; Walcholtz, W. F. *J. Phys. Chem.* **1988**, *92*, 6202.
(63) Comparison with the values obtained by Furue, *et al.*[38] for the $(bpy)_2Ru(Mebpy(CH_2)_nMebpy)Os(bpy)_2^{4+}$ (n = 2, 3, 5, 7) compounds may have little significance because of the lack of rigidity of such compounds. We only notice that the value obtained (5.0×10^7 s^{-1}) for Ru^{II}·A·Os^{II}, where the center-to-center separation distance is 17 Å, is smaller than that (8.1×10^7 s^{-1}) obtained for the compound with $n = 7$ of the Furue series (center-to-center separation distance assumed to be that of the fully extended *trans* conformation, 18.6 Å). This suggests that the effective distance in Furue's compound may be smaller than that of the fully extended structure.
(64) Balzani, V.; Bolletta, F.; Scandola, F. *J. Am. Chem. Soc.* **1980**, *102*, 2552.
(65) Scandola, F.; Balzani, V. *J. Chem. Educ.* **1983**, *60*, 814.
(66) Marcus, R. A. *Annu. Rev. Phys. Chem.* **1964**, *15*, 155.
(67) Sutin, N. *Acc. Chem. Res.* **1982**, *15*, 275.
(68) The rate of energy transfer via a Coulombic mechanism in $*Ru^{II}$·A·Os^{III} and $*Ru^{II}$·A·Ru^{III} can be ruled out because the value of the overlap integral (eq 6) is very small.

Table IV. Experimental Rate Constants and Related Parameters[a]

	k, s^{-1}	$\Delta G°$, eV	λ_i, eV	λ_o, eV	$\exp(-\Delta G^*/RT)$	ν, s^{-1}	H, cm^{-1}
			Electron Transfer				
$*Ru^{II}·A·Ru^{III} \rightarrow Ru^{III}·A·Ru^{II}$	1.1×10^9	−2.06	0.1	1.3	0.47	2.3×10^{10}	10
$*Os^{II}·A·Os^{III} \rightarrow Os^{III}·A·Os^{II}$	5.0×10^9	−1.71	0.1	1.3	0.51	9.8×10^9	7
$*Ru^{II}·A·Os^{III} \rightarrow Ru^{III}·A·Os^{II}$	8.7×10^9	−1.62	0.1	1.3	0.69	1.3×10^{10}	8
$Ru^{III}·A·Os^{II} \rightarrow Ru^{II}·A·Os^{III}$	1.0×10^6	−0.44	0	1.3	3.3×10^{-3}	3.2×10^8	1
			Energy Transfer				
$*Ru^{II}·A·Os^{II} \rightarrow Ru^{II}·A·*Os^{II}$	5.0×10^7	−0.35	0.2	0	0.28	1.8×10^8	0.6

[a] Classical treatment, eqs 9 and 11.

which is the electron-transfer version of the previously seen eq 7. Similarly,

$$\nu_{el} = \frac{2(H_{el})^2}{h}\left(\frac{\pi^3}{\lambda_{el}RT}\right)^{1/2} \quad (12)$$

$$\Delta G^*_{el} = \left(\frac{\lambda_{el}}{4}\right)\left(1 + \frac{\Delta G°}{\lambda_{el}}\right)^2 \quad (13)$$

The reorganization energy λ_{el} can be expressed as the sum of two independent contributions corresponding to the reorganization of the "inner" (bond lengths and angles within the two reaction partners) and "outer" (solvent reorientation around the reacting pair) nuclear modes:

$$\lambda_{el} = \lambda_{el,i} + \lambda_{el,o} \quad (14)$$

The outer reorganizational energy, which is by far the predominant term in electron-transfer processes, can be calculated by the expression[14]

$$\lambda_{el,o} = e^2\left(\frac{1}{\epsilon_{op}} - \frac{1}{\epsilon_s}\right)\left(\frac{1}{2r_A} + \frac{1}{2r_B} - \frac{1}{r_{AB}}\right) \quad (15)$$

when the reactants are considered as spheres in a dielectric continuum. In eq 15, ϵ_{op} and ϵ_s are the optical and static dielectric constants of the solvent, r_A and r_B are the radii of the reactants, and r_{AB} is the interreactant center-to-center distance. Therefore, $\lambda_{el,o}$ is particularly large for reactions in polar solvents between reaction partners which are separated by a large distance. For the dinuclear compounds studied in this work, $r_A = r_B \simeq 4.3$ Å, $r_{AB} = 17$ Å, $\epsilon_{op} = 1.81$, and $\epsilon_s = 37$.[69] Using these values, $\lambda_{el,o}$ is calculated to be ~1.3 eV. The $\lambda_{el,i}$ contribution has been estimated to be ≤0.1 eV for the electron-transfer reactions involving the excited states of these complexes.[67] Therefore, λ_{el} is calculated to be ~1.4 eV, i.e. smaller than the free energy change $\Delta G°_{el}$ of the three electron-transfer reactions. As a consequence, the rate constants of these reactions lie in the Marcus inverted region.

For the back electron transfer reaction in $Ru^{III}·A·Os^{II}$ (Figure 7b) the electronic factor should be somewhat different from that of the electron-transfer quenching reactions in $*M^{II}·A·M^{III}$. In the former case electron transfer takes place from Os^{II} to Ru^{III}, whereas in the latter, as we have seen above, an electron is transferred from a π^*-bpy orbital of the M^{II}-based excited state to the M^{III} metal ion of the other chromophoric unit. As far as the intrinsic barrier is concerned, the only difference is that the inner sphere contribution is likely close to zero for ground-state electron transfer.[67]

The values of the experimental rate constants, free energy changes, and intrinsic barriers for the energy transfer process and the four electron-transfer processes investigated in this work have been collected in Table IV, where the calculated electronic factor ν_{el} (eq 11) and electronic interaction energy H_{el} (obtained from eq 12) have also been reported. One can see that the interaction energy is practically constant for the three "homogeneous" $*Ru^{II}·A·Ru^{III} \rightarrow Ru^{III}·A·Ru^{II}$, $*Os^{II}·A·Os^{III} \rightarrow Os^{III}·A·Os^{II}$, and $Ru^{II}·A·Os^{III} \rightarrow Ru^{III}·A·Os^{II}$, processes, while it is considerably smaller for the back $Ru^{III}·A·Os^{II} \rightarrow Ru^{II}·A·Os^{III}$ reaction, as expected on the basis of chemical intuition (vide supra). Figure 8 shows a log k_{el} vs $\Delta G°$ plot for the four electron-transfer processes investigated in this work. A Marcus-type curve obtained from the classical eq 11 by using the parameters $\lambda_{el} = 1.4$ eV and $H_{el} = 8$ cm^{-1} is also shown. As one can see, the fitting is not fully satisfactory even in the case of the three homogeneous excited-state electron-transfer processes *b*, *c*, and *d*. It is well-known, in fact, that the classical treatment neglects the role played by high-energy frequency vibrations as accepting modes. The semiclassical eq 16[14] has often been used[5-8] to express the nuclear factor in order to better fit the experimental results. Taking $\lambda_0 = 1.3$ eV,

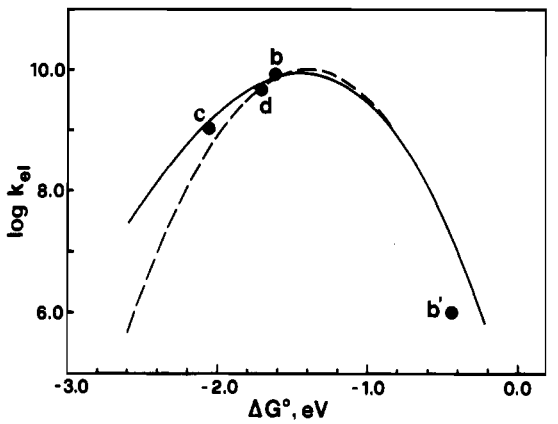

Figure 8. Log k_{el} vs $\Delta G°$ for the electron transfer reactions. Key: *b*, *c*, and *d*, indicate the k_{el} values found for the excited-state electron-transfer processes shown in Figure 7b–d, respectively; b′ indicates the value found for the back-electron-transfer reaction shown in Figure 7b. The dotted curve has been obtained by using the classical Marcus treatment (eq 11). The full line curve corresponds to the semiclassical treatment based on eq 16.

$$\mathrm{FCWD} = \frac{1}{(4\pi\lambda_0 RT)^{1/2}} e^{-S} \sum_m \frac{S_m}{m!} \exp\left[-\frac{(\Delta G° + \lambda_0 + m h\nu_i)^2}{4\lambda_0 RT}\right] \quad (16)$$

$$S = \lambda_i / h\nu_i$$

$H = 8$ cm^{-1}, and the average values $h\nu = 1400$ cm^{-1} and $S = 1.25$[70] the full line curve of Figure 8 has been obtained. As one can see, the fitting is good for the three homogeneous excited-state electron-transfer processes *b*, *c*, and *d*, whereas point *b*′, which corresponds to the back electron transfer reaction in the $Ru^{II}·A·Os^{III}$ system (Figure 7b) cannot be fit because of the different electronic factor (Table IV).

(69) The reported ϵ_{op} and ϵ_s values are for acetonitrile. Our experiments have been carried out either in 10:1 acetonitrile–water or in 40/60 acetonitrile–water. Using the ϵ_{op} and ϵ_s values of these mixtures would not cause substantial changes.

(70) For $Ru(bpy)_3^{2+}$: $h\nu = 1400$ cm^{-1}; $S = 0.95$.[71] For $Os(bpy)_3^{2+}$ $h\nu = 1390$ cm^{-1}; $S = 1.47$.[28b]

(71) Rillema, D. P.; Blandon, C. B.; Shaver, R. J.; Jackman, D. C.; Boldaji, M.; Bundy, S.; Worl, L. A.; Meyer, T. J. *Inorg. Chem.* **1992**, *31*, 1600.

Table IV also shows that the electronic interaction for the energy transfer process is much smaller than the interaction for electron transfer. This is in agreement with current theories[5,8] which predict for both electron transfer and exchange energy transfer a $k = k_0 \exp[-\beta(r - r_0)]$ dependence on distance, with the β coefficient for the energy-transfer process being twice that for electron transfer.

While any comparison with the values of the electronic interaction energies obtained for other systems[5,10,29,38] is useless because of differences in the nature of the donor, acceptor, and/or bridge, we would like to notice that the finding of an electron-transfer quenching in the $^*Os^{II}\cdot A\cdot Os^{III}$ species is at first sight in contrast with the lack of quenching observed in styrene–chloromethylstyrene polymer containing appended Os(II) and Os(III) bipyridine complexes.[28d] It should be considered, however, that such apparently similar systems are in fact quite different for the following reasons: (i) the through-bond distance between adjacent Os^{II} and Os^{III} species in the polymer system is much longer than that in $Os^{II}\cdot A\cdot Os^{III}$, so that the through-bond interaction is much smaller; (ii) for electron transfer in encounters between appended units in the polymer system, the electronic interaction will be more favorable but the reorganizational barrier will be much higher because of the short intercomponent distance and a likely less polar environment. This can place the reaction in a deeper Marcus inverted region.

Conclusions

We have prepared the novel rigid bridging ligand 1,4-bis[2-(2,2′-bipyridin-5-yl)ethenyl]bicyclo[2.2.2]octane (bpy–S–bpy, Figure 1), where the spacer S is 9 Å long. The mono and binuclear complexes $(bpy)_2Ru(bpy–S–bpy)^{2+}$ ($Ru^{II}\cdot A$), $(bpy)_2Os(bpy–S–bpy)^{2+}$ ($Os^{II}\cdot A$), $(bpy)_2Ru(bpy–S–bpy)Ru(bpy)_2^{4+}$ ($Ru^{II}\cdot A\cdot Ru^{II}$), $(bpy)_2Os(bpy–S–bpy)Os(bpy)_2^{4+}$ ($Os^{II}\cdot A\cdot Os^{II}$), and $(bpy)_2Ru(bpy–S–bpy)Os(bpy)_2^{4+}$ ($Ru^{II}\cdot A\cdot Os^{II}$) have been prepared and their absorption spectra, luminescence properties, and electrochemical behavior have been investigated. In the dinuclear compounds, the absorption spectrum and redox potentials of each metal-based unit are unaffected by the presence of the other unit. In the $Ru^{II}\cdot A\cdot Os^{II}$ compound, photoinduced energy transfer from the Ru^{II}-based to the Os^{II}-based luminescent ^{3}MLCT levels takes place with a rate constant of 5.0×10^7 s^{-1}, which is somewhat larger than the calculated value for a dipole–dipole (Förster-type) energy-transfer mechanism. If an exchange energy-transfer mechanism is assumed, the value of the electronic matrix element is observed to be ~ 0.6 cm^{-1}. Partial oxidation of the $Ru^{II}\cdot A\cdot Ru^{II}$, $Ru^{II}\cdot A\cdot Os^{II}$, and $Os^{II}\cdot A\cdot Os^{II}$ species leads to the mixed-valence compounds $Ru^{II}\cdot A\cdot Ru^{III}$, $Ru^{II}\cdot A\cdot Os^{III}$, and $Os^{II}\cdot A\cdot Os^{III}$ where light absorption by the M^{II}-based unit is followed by deactivation via strongly nonadiabatic electron-transfer processes which lie in the inverted free-energy region ($k_{el} = 1.1 \times 10^9$, 8.7×10^9, and 5.0×10^9 s^{-1}, respectively). The electronic matrix element for these nonadiabatic electron-transfer processes is 7–10 cm^{-1}. In the case of $^*Ru^{II}\cdot A\cdot Os^{III}$, the electron-transfer quenching process leads to the $Ru^{III}\cdot A\cdot Os^{II}$ intervalence transfer isomer, which then relaxes to the thermodynamically stable $Ru^{II}\cdot A\cdot Os^{III}$ species by a strongly nonadiabatic, activated electron-transfer process ($k_b = 1.0 \times 10^6$ s^{-1}). The experimentally observed rate constants for the electron-transfer processes constitute a consistent set of values that can be interpreted in the frame of current theories.

Acknowledgment. We would like to thank Elena Bagli for her help in experimental measurements, L. Minghetti for technical assistance, and G. Gubellini for the drawings. This work was supported by MURST and the CNR (Italy), the Swiss National Science Foundation (Switzerland), and "Bundesministerium fur Forschung und Technologie", Project No. 0329120 A (Germany).